Physica C 197 (1992) 251–260
North-Holland

PHYSICA C

Electronic structure of single crystal C_{60}

J. Wu, Z.-X. Shen, D.S. Dessau, R. Cao, D.S. Marshall, P. Pianetta and I. Lindau
Stanford Synchrotron Radiation Laboratory, Stanford, CA 94309, USA

X. Yang, J. Terry, D.M. King and B.O. Wells
Stanford Electronics Laboratories, Stanford, CA 94309, USA

D. Elloway, H.R. Wendt, C.A. Brown, Heinrich Hunziker and M.S. de Vries
IBM Research Division, Almaden Research Center, San Jose, CA 95120-6099, USA

Received 24 April 1992

We report angle-resolved photoemission data from single crystals of C_{60} cleaved in UHV. Unlike the other forms of pure carbon, the valence band spectrum of C_{60} consists of many sharp features that can be essentially accounted for by the quantum chemical calculations describing individual molecules. This suggests that the electronic structure of solid C_{60} is mainly determined by the bonding interactions within the individual molecules. We also observe remarkable intensity modulations of the photoemission features as a function of photon energy, suggesting strong final state effects. Finally, we address the issue of the band width of the HOMO state of C_{60}. We assert that the width of the photoemission peak of C_{60} does not reflect the intrinsic band width because it is broadened by the non 0–0 transitions via the Franck–Condon principle. Our view point provides a possible reconciliation between these photoemission data and those measured by other techniques.

1. Introduction

Buckminsterfullerene, a newly discovered form of pure carbon, is a molecule with 60 carbon atoms that occupy the 60 vertices formed by the intersections of 20 hexagonal and 12 pentagonal faces to form a hollow cage, as depicted in fig. 1. Due to the beauty of its highly symmetric structure, C_{60} has attracted much attention.

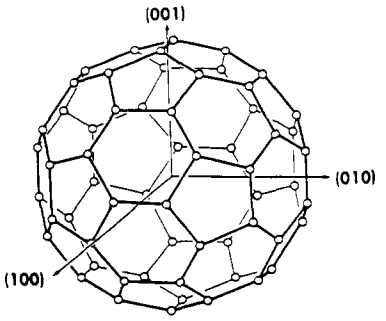

Fig. 1. Illustration of C_{60} molecular structure.

Theoretical conjectures of C_{60} clusters date back twenty years [1,2], and fullerene C_{60} was first identified in carbon vapor produced by laser irradiation of graphite in 1985 [3]. It was not until very recently that large quantities of C_{60} became available, which made it possible to discover the high-temperature superconductivity in alkali doped C_{60} [4–6], and to observe the large non-linear optical response [7]. These and other interesting properties of C_{60} stimulated research activities over the past two years [8]. By now, much effort has been made to carry out various experiments that reveal the geometric structure [9,10], the transport characteristics [11], and electronic structure [12–16], among other properties of this novel form of carbon. Theoretical calculations predict that C_{60} is a semiconductor with a direct gap of 1.5 eV [17].

Unlike graphite and diamond, solid C_{60} is a molecular crystal. The C–C bonds within an individual

C_{60} molecule are 1.4 Å and 1.46 Å long. This length is significantly shorter than the smallest C–C nearest neighbour distance between the molecules, which is about 3 Å. Although the C–C bond within the C_{60} molecule is shorter than the bond in graphite (1.42 Å and 3.4 Å) and diamond (1.54 Å), its density is smaller than both graphite and diamond (see fig. 2 for crystal structures [18]). This leads us to a model of the solid C_{60} that is comprised of well-separated C_{60} molecules, which each consists of 60 tightly bonded carbon atoms. An understanding of this unique crystal structure is essential in order to interpret the electronic structure.

In this paper, we present results of our experimental studies of C_{60} single crystals. We focus on two primary issues:
(1) the electronic structure as mainly determined by the bonding interactions within individual molecules;
(2) the band width as induced by electron hopping between the C_{60} molecules. These issues are important for the understanding of many interesting properties of the fullerenes. We show that the valence band spectrum of C_{60} exhibits many sharp features, and can be very well accounted for by the electronic states of the individual molecule with small modifications due to the band effects in the solid. This is in contrast to the spectra of graphite and diamond, which show broad features due to the large energy dispersion. Furthermore, we observe very strong intensity modulations of the photoemission features as a function of photon energy. This intensity modulation is indicative of final state effects, suggesting that one should be very careful in interpreting the photoemission data of C_{60}.

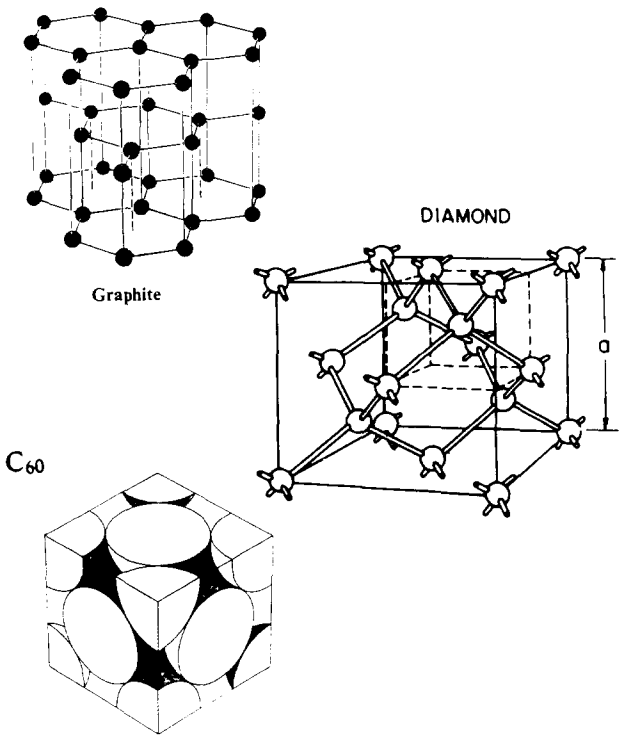

Fig. 2. Crystal structure of C_{60} together with the crystal structures of other pure forms of carbon: graphite and diamond.

The conducting band width is an important issue for a theoretical understanding of the mechanism of superconductivity. Due to the repulsive nature of the electrons, a narrow band does not favor the traditional electron–phonon coupling mechanism. The experimental results of the band width are presently controversial. Measurements such as IR reflectivity, NMR, critical field, and magnetic susceptibility give band widths of about 80–200 meV [19–23]. This range of band width values was obtained indirectly from the density of states measured in these experiments. Contradicting these results, the peak widths for both the highest valence band state and the lowest conduction band state range from 800 meV to 1200 meV in the existing photoemission spectra from polycrystalline samples [12–16]. These values of the photoemission peak widths are significantly larger than the energy resolution in the experiments which are typically of the order of 100 to 200 meV. If these values from photoemission data are taken as the band widths [14], then the photoemission results and the results obtained by other measurements differ by about an order of magnitude. We performed the first angle-resolved photoemission experiments on single crystal C_{60} to address the issue. We found that although the first valence band peak has a width of about 800 meV, it disperses by as little as 50 meV even with substantial changes of electron crystal momentum. From an analysis of our result and the gas phase data in the literature, we conclude that the peak width one measures from photoemission data may be dramatically modified by final state effects, and thus may not reflect the true band width which is substantially narrower. We further suggest that the band width of the system is much narrower than the

PES peak width. This observation provides a possible reconciliation between earlier photoemission results and those obtained by other measurements.

2. Experimental

C_{60} was produced by the carbon arc method [10], followed by toluene extraction and chromatographic separation. The resulting material was freed from solvent by heating at 250°C in a quartz tube at 10^{-7} Torr vacuum, followed by sublimation at 450°C. From this material, small crystals, typically 50 micron in size, were sublimed in a sealed tube with a small temperature gradient. These small crystals were placed in a new tube and once again baked at 120°C for about 10 h, while pumping at an active vacuum of 10^{-7} Torr. Again the tube was sealed off and this material was used to grow larger crystals by condensation out of the vapor phase. High resolution TEM micrographs and electron diffraction of crystals grown by this method showed them to have either fccd or hcp structures, and stacking faults were sometimes observed [24]. The quality of the single crystal samples has been verified by transmission Laue pattern, as shown in fig. 3. The Laue pattern was obtained with the X-ray beam perpendicular to the cleaved surface plane. We typically obtain two types of diffraction patterns, showing clear diffraction spots in three- or six-fold symmetry, respectively. These diffraction patterns do not have any stripes, implying that the samples indeed are high quality single crystals. We believe that the three-fold Laue pattern is taken along (111) directions of a fcc crystal, while the six-fold Laue pattern is taken (0001) directions from a hcp crystal. Although a fcc structure with stacking fault may also give a six-fold pattern, this stacking fault must be ordered. It is important to note that a Laue pattern is different from a mono-energetic high energy electron diffraction pattern. In real space, the crystals also appear to be different with one showing triangular facies and the other showing hexagonal facies. We have performed angle-resolved photoemission measurements on both types of sample, and the experimental results are qualitatively the same as we will discuss later.

The photoemission study of C_{60} was performed in a VG ADES 400 system with a hemispherical energy analyzer at the TGM beam line I-2 of the Stanford Synchrotron Radiation Laboratory. The base pressure of the chamber during the experiment was 2×10^{-10} Torr, and the overall energy resolution was about 200 meV. An irregularly shaped single crystal of C_{60} was cemented to a post, and then another post

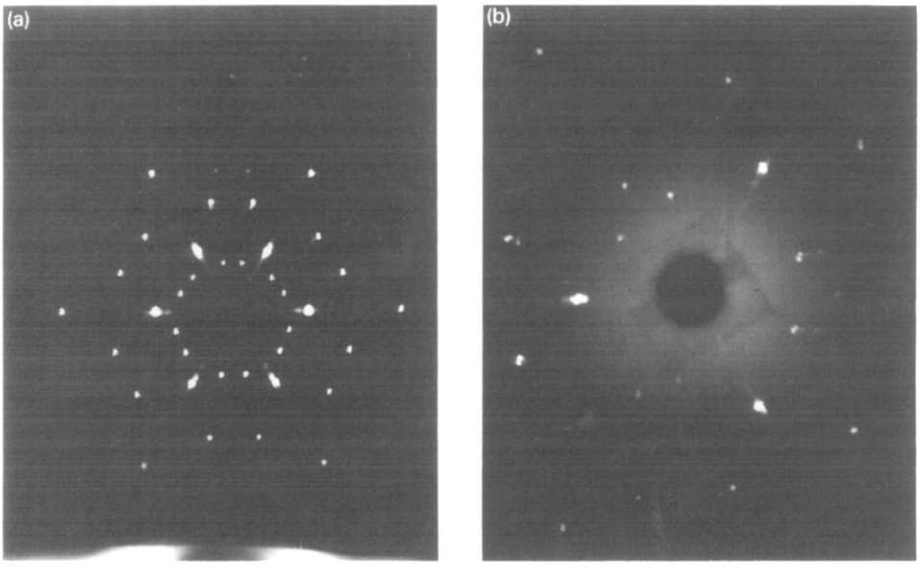

Fig. 3. Transmission Laue pattern along a cleaved direction of the C_{60} single crystal.

("top post") was cemented to the top of the sample. The samples on the holder were then introduced into the UHV chamber through a fast entrance load-lock and cleaved in situ by knocking the top post off at room temperature. The surface areas of the cleaved crystals range from 0.2 mm^2 to 0.3×0.4 mm^2, which were large enough for our photoemission experiment albeit with a limited counting rate. Due to their semiconducting nature, the sample showed some charging, but it was controlled by coating the sides of the sample with a conductive material, shining low energy electrons on the sample with a flood gun, and controlling the intensity of the synchrotron light. The data reported here were collected after the charging had stabilized.

3. Results and discussions

3.1. Valence band spectra and comparison with that of graphite and diamond

Figure 4 shows two photoemission spectra recorded at normal emission with photon energies of 60 and 100 eV, respectively. These spectra are very similar to data taken from polycrystalline C_{60} films [13–16]. As we will discuss in detail later, we find no evidence of a sizable energy dispersion. For comparison, we have also included in fig. 4 angle-integrated spectra from graphite [25] and diamond [26]. The valence band spectra of graphite and diamond consist of broad features from dispersive bands. In contrast, the photoemission data from C_{60} crystals exhibit very distinct valence band features as marked. These valence band features actually originate from the molecular states that are not significantly modified by energy dispersion in C_{60} crystal. This point is very clear from a comparison of our experimental data with the results of a molecular cluster calculation represented by vertical bars in fig. 4 [17]. We can see that the data agree remarkably well with the cluster calculation, indicating that the electronic structure of the C_{60} crystal is mainly determined by the molecular bonding of the individual C_{60} molecules, and the effect of the energy dispersion is relatively small. This assertion also receives very strong support from the fact that photoemission spectra from a solid film and from a gas phase are very similar. [12]. The gas phase photoemission data are completely determined by the bonding of individual C_{60} molecules. This result is not surprising, since according to the crystal structure as depicted in fig. 2, the bond length of two carbon atoms in adjacent molecules is almost 3Å which is much longer than the atomic distance within a molecule (1.4 Å). Therefore, the intra-molecular bonding dominates the electronic structure.

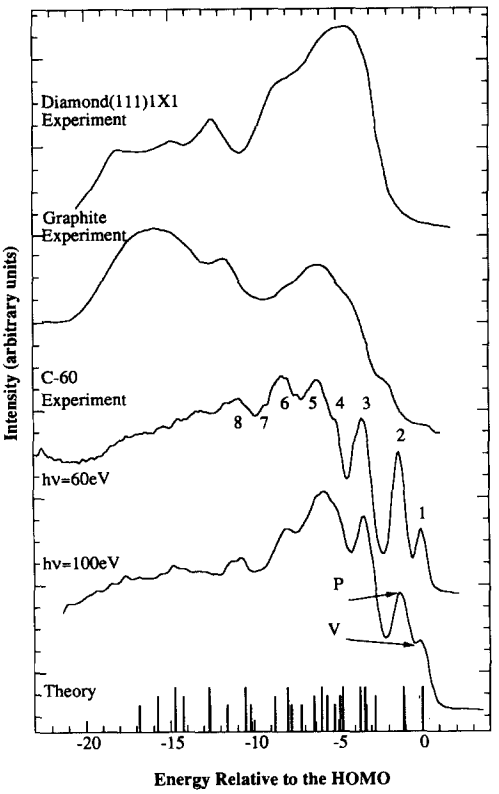

Fig. 4. Valence band spectra of C_{60} together with that of graphite and diamond.

The difference between the spectra of C_{60} and that of graphite and diamond can be understood from the crystal structure in fig. 2. The bands in graphite derive mainly from the sp^2 bonds determined by the in-plane bond length of 1.42 Å and the free-electron-like π-bonds. The bands of diamond derive mainly from the sp^3 bonds with an interatomic bond length of 1.54 Å. Because of the relatively short atomic distances involved in graphite and diamond, there is large wave function overlap and these bands are very

dispersive, resulting in broad valence band features in fig. 4. The bonding of C_{60} is a mixture of sp^2 and sp^3 hybrids. However, the energy dispersion of C_{60} is determined by the ~ 3 Å bond length in adjacent molecules. Because of this significantly larger bond length, the energy dispersion is much smaller.

3.2. Photon energy dependence of the valence band spectra

The above discussion leaves us with the general picture that the electronic structure of C_{60} as measured by photoemission is mainly determined by the molecular states, with small modifications due to the formation of narrow bands in the solid. In this section, we report interesting intensity modulations of the photoemission spectra as a function of photon energy. This dramatic photon energy dependence of the photoemission intensity suggests the fact that the photoemission final state (or intermediate resonance state) retains much of the molecular character of C_{60}, and the final state effects are important to understand the photoemission data.

Figure 5 shows EDC spectra of a C_{60} crystal taken at various photon energies. The intensity of the C_{60} valence band features modulates dramatically with the photon energy. For example, the intensity of feature 1 shows a minimum at 35 eV, and a maximum at 47.5 eV, but the intensity of feature 2 reaches opposite extremes at these photon energies. This photoemission intensity modulation is likely to be related to final state effects.

To further investigate the matter, we performed a more detailed study on this issue using the constant initial-state spectroscopy (CIS) technique. The CIS technique was first employed by Lapeyre et al. for a measurement of the density of final states of KCl [27]. In this type of spectroscopy, electrons from the same initial-state energy are excited to different final-state energies by a synchronous scanning of photon energy and the pass energy of the electron analyzer. Figures 6 and 7 show the CIS scan of the C_{60} crystal. These spectra were normalized by the mesh current monitoring the photon beam intensity from the monochromator. The initial state energy (E_i) labeled in the figures is relative to the highest occupied molecular orbital. Besides the primary photoemission process, secondary processes such as electron–electron scattering, contribute to the EDC spectrum. To separate the primary process from the secondary processes in the CIS data, all the spectra presented in fig. 7 are obtained in the following method: two CIS spectra (see fig. 6) were obtained from the peak (P) and the valley (V) at higher kinetic energy as indicated in fig. 4. The CIS-P is the spectrum excited

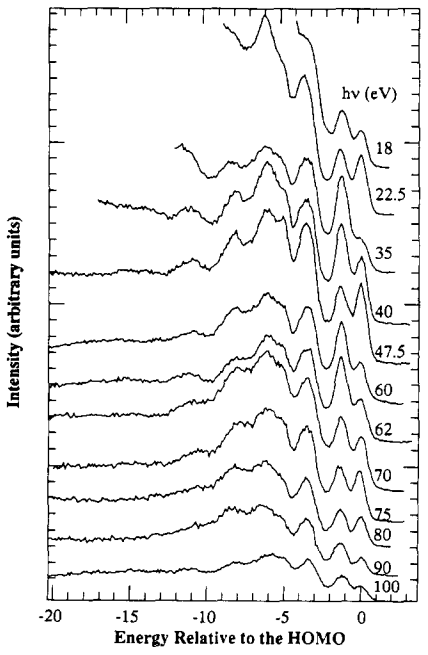

Fig. 5. Valence band spectra of C_{60} recorded with different photon energies.

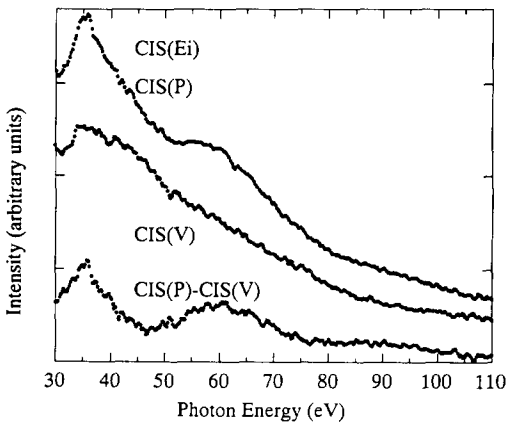

Fig. 6. Illustration of background subtraction procedure in CIS data.

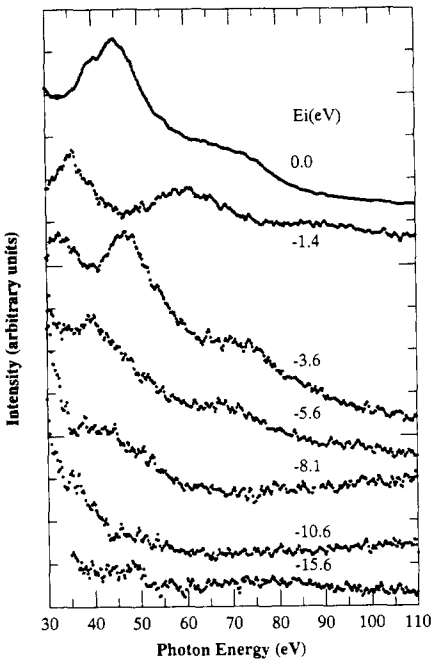

Fig. 7. CIS spectra with different initial energies corresponding to the peaks in C_{60} valence band spectra.

from the initial-state at the peak of the EDC spectrum, and the CIS-V is the spectrum excited from the state in the valley of the EDC spectrum that is mainly from the secondary processes. The bottom curve CIS (E_i) is obtained by subtracting the CIS-V from CIS-P to eliminate the background emission.

Figure 7 presents a stack of CIS spectra excited from the peaks of the valence band EDC curves after subtracting the background emission. The initial-state of the topmost curve is the HOMO state, and the initial state of the second curve is the second highest occupied state. A previous study of polycrystalline thin film reported only the first two curves, and the way to normalize the data in that paper is also different from ours [28]. The authors of the earlier paper normalized the intensity of features 1 and 2 to that of feature 4. We can see the upper three curves show strong intensity variation with photon energy, which are very different from the carbon atomic photoionization cross section and the graphite data [25]. Furthermore, these intensity modulations of different photoemission features exhibit very clear anti-phase relations. For example, the first peak reaches a maximum at the same photon energy for which the second peak reaches a minimum. The bottom three curves, excited from the deeper C_{60} valence band feature, attenuate with photon energy monotonically. Part of this lack of structure is probably due to difficulties in subtracting the secondary electrons from these features at higher binding energies. It is clear that the CIS curve excited from peak 4($E_i = -5.6$ eV) shows intensity modulation too. This shows that the assumption in the earlier paper that this feature should exhibit no intensity modulation because of the mixed nature of π and σ bonds is only a crude approximation [28].

The interesting phase relation of the intensity modulations of the first three features is probably related with some sort of symmetry selection rules. Because the hollow cage structure of C_{60} is very close to a sphere, the molecular orbitals may be crudely characterized by the angular momentum quantum number l. The angular part of the wave function is defined by the spherical harmonic function $Y_{lm}(\vartheta, \phi)$. The energy of the state is proportional to $l(l+1)$ with a degeneracy of $2l+1$. The states with even l have even symmetry and those with odd l have odd symmetry. The C_{60} molecule belongs to the icosahedral point group, and using group theory we can determine the allowed transitions between the states. The highest occupied molecular orbital (HOMO) of the C_{60} valence band corresponding to the $l=5$ π-derived state, has an odd symmetry, and the second feature corresponds to the $l=4$ π-derived state, and has an even symmetry [29]. According to parity selection rules, if the transition between the peak 1 state and a final state is allowed (enhancing the intensity of the CIS curve), then the transition between the peak 2 state and the same final state is forbidden (suppressing the intensity of the CIS curve) (note, check feature 3). While we can have a qualitative understanding of the intensity modulation from the above simple analysis, a more detailed calculation based on the above model and free-electron-like final states show much more oscillation than the experimental results. We thus suggest that the final states of C_{60} well above the vacuum level retain much of the molecular character, and we would like to see more sophisticated theoretical calculations ot understand this interesting intensity modulation.

The remarkable intensity modulations discussed in this section, and shown in figs. 5–7, suggest that the final state effects are very strong in C_{60}, and one has to be cautious in interpreting photoemission data from this system. This leads us to the issue of the band width of C_{60}. As discussed in the introduction, some earlier photoemission data were interpreted to give a band width that is an order of magnitude larger than the results of other experiments. In the next section, we will show that the final state effects (not necessarily in the same sense as those discussed in this section, rather of vibronic nature) actually make the interpretation of photoemission data a very complicated task, and the photoemission peak width does not simply reflect the band width as was interpreted previously [14].

3.3. Angle-resolved photoemission and its implication for the band width

As we have indicated in the introduction, the issue of the energy band width is very important for the understanding of many properties of solid C_{60}, in particular the mechanism of superconductivity. Angle-resolved photoemission experiments have been a very powerful tool to study the band width of solids since they directly reveal the energy versus momentum information. In this section, we use angle-resolved photoemission as a tool to address the issue of the C_{60} band width. The experimental data from both the normal and off-normal emission were mainly collected along high-symmetry directions.

Figure 8 presents two complementary sets of angle-resolved photoemission data from a single crystal of C_{60} cleaved in ultra-high vacuum. Panel (a) gives off-normal emission data with a photon energy of 25 eV, while panel (c) gives normal-emission data at various photon energies. In the normal-emission case, we fixed the direction of the $\boldsymbol{k}$ vector but changed its amplitude. In the off-normal emission case, we fixed the amplitude of the $\boldsymbol{k}$ vector but changed its direction. In both cases, we change the $\boldsymbol{k}$ vector by relatively small amounts. However, this change is very sizable as compared to the small Brillouin zone size of the C_{60} crystal (approximately 60% and 20% for the off- and normal emission cases, respectively) [30]. To first order, the most obvious conclusion from fig. 8 is that, although the photoemission feature of C_{60} has a sizable width, there is minimal energy dispersion of the features, i.e., the photoemission features do not move with the change of emission angle or photon energy. The upper bound for the energy dispersion of the first and second photoemission features is 50 meV which is shown more clearly in panel (b). We notice that the first photoemission feature (HOMO) shifts by 50 meV at a 6° emission angle, and then shifts back by about 20 meV at a 9° emission angle. The experimental conditions during the data collection were very stable and we reproduced the normal emission data after we took the off-normal emission data. Therefore, we believe that the experimental observation is real. However, we cannot rule out the possibility that this small shift is caused by a change in the spectral background, or that each photoemission feature contains several states and their relative intensity may change with emission angle and photon energy. In any case, we

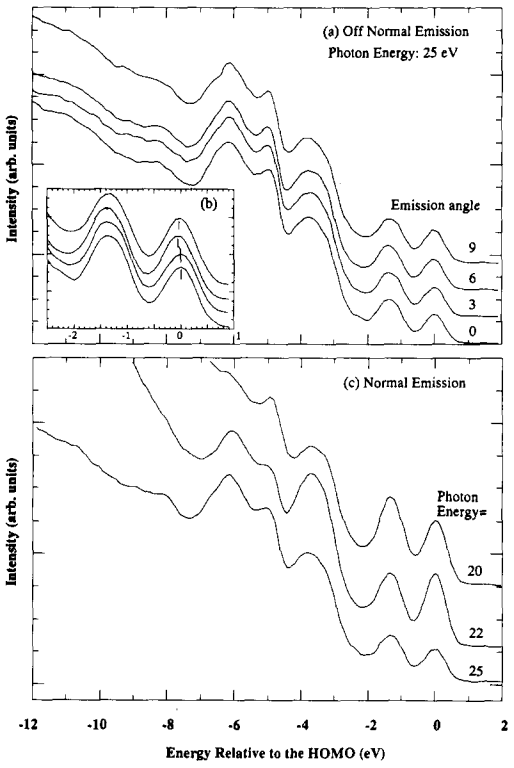

Fig. 8. (a) Off-normal emission data from the C_{60} single crystal; the inset (b) shows details of the first two photoemission peaks. (c) Normal-emission data from the C_{60} single crystal.

are confident to say that the energy dispersions of the C_{60} photoemission features are very small, and 50 meV is the upper bound.

Hence, our angle-resolved data provide the following picture: although the photoemission feature width is much wider than our experimental resolution, we see neither a sizeable energy dispersion nor a sizable change of the photoemission peak width with substantial changes of crystal momentum. This result puts further constraints on the width of the energy bands. The lack of energy dispersion in the photoemission features of this compound does not necessarily mean that there are no dispersions of individual bands. All the photoemission features resolved contain several bands (e.g., the first feature is fivefold degenerate), and the individual bands may disperse differently. We might have a situation that the individual bands have some dispersion while the centroid of these bands is basically non-dispersive. This scenario leads to a change of the width of the photoemission features; however, since we did not see any sizable changes of the widths of photoemission features, we think the dispersion of individual bands is also small. Another possible explanation for the lack of energy dispersion in our data is the rotational disorder. It has been found that the C_{60} molecules spin with high frequencies in the solid [19]. The hopping matrix elements and therefore the band width will be affected by the relative orientations of the C_{60} molecules. Nevertheless, the rotational disorder alone cannot explain why the photoemission features observed are much broader than the instrumentational resolution. A completely disordered system naturally gives narrow bands. Furthermore, since the trend (say, upwards or downwards) of the energy dispersion in a C_{60} solid is determined by the crystal structure, the rotational disorder of the individual molecules may produce many bands with different widths but the same trend. We may still see the "averaged energy dispersion" of these bands if some of them are very dispersive. Hence, our data may not be easily explained by rotational disorder alone.

The above discussion makes it very clear that the width of the photoemission feature in C_{60} does not reflect the band width of solid C_{60}. The band width of C_{60} is likely to be much narrower than the width of the photoemission feature, even though it is difficult to pin down exactly how narrow the real band width is. This assertion is different from an earlier interpretation of the photoemission data [14]. Now the question that must answered is: how does broadening of the photoemission peak arise? The instrumentational resolution is not the main cause of the broadening since the typical photoemission experimental resolution is much better than the peak width. Although another traditional cause for a peak broadening is due to the photo-hole lifetime, here we are dealing with either the highest valence band state or the conduction band state, and so the quasi-particles are expected to have a long lifetime. Hence our data cannot be explained by the photo-hole lifetime broadening. The rotational disorder cannot explain it since it naturally gives narrow bands. Thus, other reasons for the broadening of the photoemission spectra must exist.

An important point to remember in interpreting photoemission data is that photoemission is an excited state measurement. The final state effect in the photoemission process could introduce additional complications. In fact, precedents of final state broadening of photoemission features have been observed in other materials before. For example, the very sharp exciton state of F-centers in KI appeared in the photoelectric emission data to have a width of approximately 1 eV at room temperature [31]. The broadening of the exciton state in F-centers was explained by the Franck–Condon final state effect [32]. Figure 9 depicts the photoemission process and the

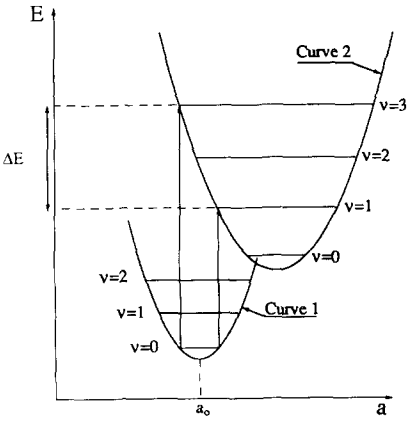

Fig. 9. Illustration of photoemission process and mechanism of the final state broadening.

broadening mechanism of the photoemission feature via the Franck–Condon principle. Curves 1 and 2 represent the system energy as a function of some generalized coordinate for the ground state and the excited state, respectively. We start out in the system energy curve 1 with an equilibrium position a_o. In the photoemission process, because of the charge redistribution, the system energy also has to be changed, and we end up the curve 2. Because the photoemission process is much faster than the speed of the ion movements, all photoemission transitions are vertical transitions. Depending on the shape of curve 2, the spectral width ΔE may be broadened. Such broadening is significant only if there are appreciable changes of equilibrium positions of the final state. Without an appreciable change of the final state geometry, the optical transition is dominated by the 0–0 transition ($n=0$ vibrational state in curve 1 to $n=0$ vibrational state in curve 2). If we allow an appreciable change of the geometry in the final state, non 0–0 transitions become possible via the Franck–Condon principle, and they will have significant oscillator strength. These non 0–0 transitions are usually in the steep part of the curve 2, resulting in large ΔE.

A key for such a broadening effect to happen in the F-centers is the localized nature of the system. The photo-hole is local enough to cause enough change of local geometry and thus the system energy curve as depicted in fig. 3. Since the photo-hole left in the HOMO is distributed in the entire molecule, one would not start out expecting a very large lattice distortion. Although it is quite reasonable to believe that the photo-hole is localized within a C_{60} molecule, it is still distributed over 60 carbon atoms. Hence, there is no clear prior reason to believe in a large non 0–0 transition in this system. This is consistent with the theoretical calculation that the relaxation energy of the molecule is small [33]. The way one can definitively answer this question is to perform experiments on C_{60} molecules. Fortunately, such studies from gas phase C_{60} have been performed by Lichtenberger et al. [12] and Baltzer et al. [34]. These studies show that the photoemission spectra from gas phase are also very broad, and thus unambiguously establish that the photoemission spectra have been broadened by reasons other than energy dispersion. With an exceptionally good energy resolution of 22 meV, Baltzer et al. can resolve three features for the highest molecular orbital state (HOMO) [34]. Since HOMO is a mono-energetic state, the three resolved features have to be the vibrational states and the non 0–0 transitions have to be strong. Similarly, we expect vibrational final state effects important to the photoemission data from the solid.

Therefore, we are left with the following picture: the band dispersion in solid C_{60} is quite small, and a significant part of the broadening in the photoemission spectra comes from non 0–0 transitions to excited vibrational final state. This observation provides a possible account for why the band width as determined by photoemission is an order of magnitude larger than that determined by other measurements such as NMR, susceptibility, and IR reflectivity. We suggest that the peak width one measures from photoemission data may be dramatically modified by final state effects, and thus may not reflect the true band width that is substantially narrower.

4. Conclusions

In summary, our photoemission spectra from single crystal C_{60} show sharp molecular features, indicating the molecular orbitals are relatively undisturbed in solid C_{60}. We observed interesting intensity modulations of the valence band features as a function of the photon energy, indicating strong final state effects. Our angle-resolved photoemission data reveals the C_{60} single crystal has narrow bands that exhibit minimal energy dispersion. We suggest that the band broadening may be caused by the non 0–0 transition to excited vibrational final states. This result reconciles the controversy about the band width of the C_{60} as measured by different techniques.

Acknowledgements

We acknowledge the helpful discussions with Dr. W.E. Spicer and Dr. W.A. Harrison. This research was performed at the Stanford Synchrotron Radiation Laboratory (SSRL) which is operated by the Department of Energy, Office of Basic Energy Sciences, Divisions of Chemical Sciences. The office's

Division of Materials Sciences has provided support for this research.

References

[1] E. Osawa, Kagaku, 25 (1970) 854 (in Japanese).
[2] Z. Yoshida and E. Osawa, Aromaticity (Kagakudojin, Kyoto, 1971) p. 174 (in Japanese).
[3] H.W. Kroto, J. Heath, S.C. O'Brien, R.F. Curl and R.E. Smalley, Nature 318 (1985) 162.
[4] A.F. Hebard, M.J. Rosseinsky, R.C. Haddon, D.W. Murphy, S.H. Glarum, T.T.M. Palstra, A.P. Ramirez and A.R. Kortan, Nature 350 (1991) 600.
[5] K. Holczer, O. Klein, S.-M. Huang, R.B. Kaner, K.-J. Fu, R.L. Whetten and F. Diederich, Science 252 (1991) 1154.
[6] K. Holczer, O. Klein, G. Gruner, J.D. Thompson, F. Diederich and R.L. Whetten, Phys. Rev. Lett. 67 (1991) 271.
[7] W.J. Blau, H.J. Byrne, D.J. Cardin, T.J. Dennis, J.P. Hare, H.W. Kroto, R. Taylor and D.R.M. Walton, Phys. Rev. Lett. 67 (1991) 1423.
[8] H.W. Kroto, A.W. Allaf and S.P. Balm, Chem. Rev. 91 (1991) 1213.
[9] R.J. Wilson, G. Meijer, D.S. Bethune, R.D. Johnson, D.D. Chambliss, M.S. De Vries, H.E. Hunziker and H.R. Wendt, Nature 348 (1990) 621.
[10] W. Krätschmer, L.D. Lamb, K. Fostiropoulos and D.R. Huffman, Nature 347 (1990) 354.
[11] P.M. Allemand, G. Srdanov, A. Koch, K. Khemani and F. Wudl, J. Am. Chem. Soc. 113 (1991) 2780.
[12] D.L. Lichtenberger, K.W. Nebesny, C.D. Ray, D.R. Huffman and L.D. Lamb, Chem. Phys. Lett. 176 (1991) 203.
[13] J.H. Weaver, J.L. Martins, T. Komeda, Y. Chen, T.R. Ohno, G.H. Kroll, N. Troullier, R.E. Haufler and R.E. Smalley, Phys. Rev. Lett. 66 (1991) 1741.
[14] C.T. Chen, L.H. Tijeng, P. Rudolf, G. Meigs, J.R. Rowe, J. Chen, T.P. McCauley Jr., A.B. Smith III, A.R. McGhie, W.J. Romanow and E.W. Plummer, Nature 352 (1991) 603.
[15] G.K. Wertheim, J.E. Rowe, D.N.E. Buchanan, E.E. Chaban, E.F. Hebard, A.R. Kortan, A.V. Makhija and R.C. Haddon, Science 252 (1991) 1420.
[16] T. Takahashi, T. Morikawa, S. Sato, H.K. Yoshida, A. Yuyama, K. Seki, H. Fujimoto, S. Hino, S. Hasegawa, K. Kamiya, H. Inokuchi and K. Kikuchi, Physica C 185–189 (1991) 417.
[17] Susumu Saito and Atsushi Oshiyama, Phys. Rev. Lett. 66 (1991) 2637.
[18] Most of reports of C_{60} structure is fcc, e.g., R.M. Flemming et al., Proc. Mater. Res. Soc. (Boston, 1990), to be published.
However, C_{60} has also been reported to have hcp structure, e.g. W. Kratschmer, L.D. Lamb, K. Fostiropoulos and D.R. Huffman, Nature 347 (1990) 354. We depict the fcc structure here because most of the recent reports give this structure and there are concerns about the impurities in hcp crystals.
[19] C.S. Yannoni, R.D. Johnson, G. Meijer, D.S. Bethune and J.R. Salem, J. Phys. Chem. 95 (1991) 9.
[20] L.D. Rotter et al., preprint.
[21] R. Tycko, G. Dabbagh, M.J. Rosseinsky, D.W. Murphy, R.M. Fleming, A.P. Ramirez and J.C. Tully, Science 253 (1991) 884.
[22] A.P. Ramirez, private communication. Susceptibility and critical field measurements also yield a narrow band width (about 7 or 8 times narrower than the photoemission data).
[23] D.S. Bethune, G. Meijer, W.C. Tang, H.J. Rosen, W.G. Golden, H. Seki, C.A. Brown and M.S. de Vries, Chem. Phys. Lett. 179 (1991) 181.
[24] R. Hgeiss, C.H. Brown, O. Chapa-perez, R.J. Savoy, H.R. Wendt, D. Elloway and M.S. de Vries, J. Electron Microscopy, in press.
[25] A. Biamoni, S.B.M. Hagstrom and R.Z. Bachrach, Phys. Rev. B 16 (1977) 5543.
[26] B.B. Pate, Ph.D. Thesis, Stanford University, 1984.
[27] G.J. Lapeyre, J. Anderson, P.L. Gobby and J.A. Knapp, Phys. Rev. Lett. 33 (1974) 1290.
[28] P.J. Benning, D.M. Poirier, N. Troullier, J.L. Martins, J.H. Weaver, R.E. Haufler, L.P.F. Chibante and R.E. Smalley, Phys. Rev. B 44 (1991) 1962.
[29] J.L. Martins, N. Troullier and J.H. Weaver, Chem. Phys. Lett. 180 (1991) 457.
[30] In our estimation, we compare $\boldsymbol{k}$ to half of the fcc Brillouin zone since it is symmetric with respect to the zone center. For the normal emission case, an inner potential of 8 eV is used. This approximation will not affect our message that we have covered a sizable portion of the zone. We have additional normal emission data which give the same result.
[31] L. Apker and E. Taft, Phys. Rev. 79 (1959) 964.
[32] See, e.g., articles by M. Lax and C. Herring, in: Photoconductivity Conf. eds. R.G. Breckenridge et al. (Wiley, New York).
[33] P. Bagus, private communication.
[34] P. Baltzer, W.J. Griffiths, A.J. Maxwell, P.A. Brühwiler, L. Karlsson and N. Martensson, to be published.